FINITE ELEMENT TECHNIQUES FOR THE NUMERICAL SIMULATION OF TWO-PHASE FLOWS WITH MASS TRANSPORT

CHRISTOPH LEHRENFELD AND ARNOLD REUSKEN*

Abstract. We consider a standard sharp interface model for the fluid dynamics in a two-phase incompressible flow, combined with a convection-diffusion model for solute transport. Some important numerical challenges related to these models are discussed. We present a finite element discretization method for the solute transport model. The method is based on an Eulerian approach, i.e. computational grids are not aligned to the interface and do not follow the interface motion. The interface motion is described using the level-set technique. We treat three numerical techniques, namely the extended finite element method (XFEM) for the approximation of discontinuities, the Nitsche-method for a convenient handling of interface conditions (e.g., Henry condition) and the space-time finite element technique. The basic underlying ideas are explained. These techniques are combined and result in the space-time Nitsche-XFEM that is used for the discretization of a two-phase solute transport problem. Properties of this method are discussed. Results of numerical experiments with this method are presented.

Key words. Two-phase flow, mass transport, XFEM, Nitsche method, space-time finite element method

AMS subject classifications. 65M60, 65Z05, 76T10

1. Introduction. Two-phase incompressible flows with surface tension forces are usually modeled by either a diffusive interface or a sharp interface model. In this paper we restrict to the numerical simulation of the latter class of models. For numerical simulations based on a diffusive interface model we refer to the literature, e.g. [2, 14, 29, 1]. In systems with incompressible fluids a sharp interface model for the fluid dynamics typically consists of the Navier-Stokes equations for the bulk fluids with an interfacial surface tension force term on the right-hand side in the momentum equation. This model is combined with a convection-diffusion equation for mass transport (of a solute). We consider flow regimes with a low Reynold's number (laminar flow), a small capillary number (significant surface tension forces) and a moderate Schmidt number, such that concentration boundary layers can be resolved. We explain why these models typically have a very high numerical complexity. Such flow models can not be solved reliably and accurately by the commercial codes that are available nowadays. There is a need for more efficient and reliable numerical techniques for this class of models. The development, analysis and application of such tailor-made numerical simulation methods is an important field in numerical analysis and computational engineering science. In this paper we restrict to a certain class of finite element discretization methods for two-phase incompressible flows, which has been developed in recent years. We treat three important and rather general finite element techniques that can be used for an accurate discretization of the mass transport equation: The extended finite element method (XFEM) for the approximation of discontinuities, the Nitsche-method for a convenient handling of interface conditions (e.g., Henry condition) and the space-time finite element technique. We restrict ourselves to an explanation of the main ideas of these methods and refer to

*Institut für Geometrie und Praktische Mathematik, RWTH-Aachen University, D-52056 Aachen, Germany; email: lehrenfeld@igpm.rwth-aachen.de,reusken@igpm.rwth-aachen.de

the literature for more detailed information. Some results of numerical experiments with these methods that were obtained using the DROPS solver [7] are presented. This finite element code is specifically developed for testing, improving and validating (new) tailor-made numerical methods for the simulation of sharp interface models for two-phase incompressible flows.
The two main contributions of this paper are a discussion of major numerical challenges for this problem class and an explanation of the three above-mentioned finite element element techniques.

2. Mathematical Model.

2.1. Fluid dynamics and mass transport. We introduce a standard mathematical model for the fluid dynamics in a two-phase flow with mass transport between the bulk phases. This model is often used in the literature, e.g., [24, 28, 31, 9]. We restrict ourselves to *isothermal conditions*, *incompressible* fluids and assume that there is *no change of phase*.

The given domain $\Omega \subset \mathbb{R}^3$, contains two different immiscible incompressible phases (liquid-liquid or liquid-gas) which may move in time and have different material properties ρ_i (density) and μ_i (viscosity), $i = 1, 2$. The density and viscosity, ρ_i and $\mu_i, i = 1, 2$, are assumed to be constant in each phase. For each point in time, $t \in [0, T]$, Ω is partitioned into two open bounded subdomains $\Omega_1(t)$ and $\Omega_2(t)$, $\overline{\Omega} = \overline{\Omega}_1(t) \cup \overline{\Omega}_2(t)$, $\Omega_1(t) \cap \Omega_2(t) = \emptyset$, each of them containing one of the phases. These phases are separated from each other by the interface $\Gamma(t) = \overline{\Omega}_1(t) \cap \overline{\Omega}_2(t)$. For convenience we assume that $\Omega_1(t)$ is strictly contained in Ω, i. e., does not touch $\partial\Omega$. The normal velocity $V_\Gamma = V_\Gamma(x, t) \in \mathbb{R}$ denotes the magnitude of the velocity of the interface Γ at $x \in \Gamma(t)$ in normal direction. $\mathbf{n}_\Gamma$ denotes the unit normal on Γ pointing from Ω_1 to Ω_2. To model interfacial forces we use the following standard (Cauchy) ansatz. The interface is considered to be a 2D continuum and on each (small) connected surface segment $\gamma \subset \Gamma$ there is a contact line force on $\partial\gamma$ of the form $\boldsymbol{\sigma}_\Gamma n$. This $\boldsymbol{\sigma}_\Gamma$ is called the *interface stress tensor* and constitutive laws for $\boldsymbol{\sigma}_\Gamma$ have to be provided by surface rheology. Examples will be given in Remark 1 below. Based on the basic conservation laws of mass and momentum the following standard model (in strong formulation) for the *fluid dynamics* of a two-phase incompressible flow can be derived:

$$\begin{cases} \rho_i(\frac{\partial \mathbf{u}}{\partial t} + (\mathbf{u} \cdot \nabla)\mathbf{u}) = \operatorname{div} \boldsymbol{\sigma}_i + \rho_i \mathbf{g} \\ \operatorname{div} \mathbf{u} = 0 \end{cases} \qquad \text{in } \Omega_i(t), \quad i = 1, 2, \tag{2.1}$$

$$[\boldsymbol{\sigma}\mathbf{n}_\Gamma]_\Gamma = \operatorname{div}_\Gamma \boldsymbol{\sigma}_\Gamma \quad \text{on } \Gamma(t), \tag{2.2}$$

$$[\mathbf{u}]_\Gamma = 0 \quad \text{on } \Gamma(t), \tag{2.3}$$

$$V_\Gamma = \mathbf{u} \cdot \mathbf{n}_\Gamma \quad \text{on } \Gamma(t). \tag{2.4}$$

with the bulk phase stress tensor $\boldsymbol{\sigma}_i = -p\mathbf{I} + \mu_i\big(\nabla\mathbf{u} + (\nabla\mathbf{u})^T\big)$, i. e., we consider Newtonian bulk fluids. The vector $\mathbf{g}$ denotes an external (gravity) force. The operator $\operatorname{div}_\Gamma$ denotes the tangential divergence, cf. [9]. The notation $[\cdot]_\Gamma$ is used to denote the jump of a quantity across Γ. The assumption that there is no change of phase leads to the dynamic interface condition (2.4). Viscosity of the fluids leads to the continuity condition in (2.3). Momentum conservation in a (small) material volume that intersects the interface leads to the stress balance condition in (2.2). To make

the problem well-posed one needs suitable initial conditions for $\Gamma(0)$ and $\mathbf{u}(x,0)$ and boundary conditions for $\mathbf{u}$ or $\boldsymbol{\sigma}\mathbf{n}$ on $\partial\Omega$.

These Navier-Stokes equations model the fluid dynamics. Note that the evolution of the interface $\Gamma(t)$ is *implicitly* defined by this model.

REMARK 1. We mention three important choices for the interface stress tensor $\boldsymbol{\sigma}_\Gamma$. For an extensive treatment of constitutive models for the surface stress tensor we refer to [24]. For $x \in \Gamma$ we define the projection $\mathbf{P}(x) = I - \mathbf{n}_\Gamma(x)\mathbf{n}_\Gamma(x)^T$. The operator $\nabla_\Gamma = \mathbf{P}\nabla$ is the tangential gradient. A so-called *clean interface* model for surface tension is given by $\boldsymbol{\sigma}_\Gamma = \tau\mathbf{P}$, with a *constant* surface tension coefficient $\tau > 0$. This results in the surface force

$$\operatorname{div}_\Gamma \boldsymbol{\sigma}_\Gamma = \operatorname{div}_\Gamma(\tau\mathbf{P}) = -\tau\kappa\mathbf{n}_\Gamma \tag{2.5}$$

used in (2.2). Here κ is the mean curvature of Γ, i. e., $\kappa(x) = \operatorname{div}\mathbf{n}_\Gamma(x)$ for $x \in \Gamma$. *In the remainder of this paper we restrict to this case.* In certain systems, e.g. with surfactants, the surface tension coefficient τ can not be assumed to be constant. This then gives rise to so-called Marangoni forces and the surface tension force in (2.2) takes the more general form $\operatorname{div}_\Gamma \boldsymbol{\sigma}_\Gamma = \operatorname{div}_\Gamma(\tau\mathbf{P}) = -\tau\kappa\mathbf{n}_\Gamma + \nabla_\Gamma\tau$. A third example for the interface stress tensor is one that is used to model viscous forces in the interface. With $\mathbf{D}_\Gamma(\mathbf{u}) := \mathbf{P}\big(\nabla_\Gamma\mathbf{u} + (\nabla_\Gamma\mathbf{u})^T\big)\mathbf{P}$ the *Boussinesq-Scriven* constitutive law is given by

$$\boldsymbol{\sigma}_\Gamma = \tau\mathbf{P} + (\lambda_\Gamma - \mu_\Gamma)\operatorname{div}_\Gamma \mathbf{u}\,\mathbf{P} + \mu_\Gamma\mathbf{D}_\Gamma(\mathbf{u}).$$

The constants $\mu_\Gamma > 0$ and $\lambda_\Gamma > 0$ are called the *interface shear viscosity* and *interface dilatational viscosity*, respectively. Other examples of interface stress tensors $\boldsymbol{\sigma}_\Gamma$, e.g. for the important case of visco-elastic interfacial behavior, are treated in [25].

We assume that one or both phases contain a dissolved species that is transported due to convection and molecular diffusion and does not adhere to the interface. The concentration of this species is denoted by $c(x,t)$. A standard mathematical model for the mass transport is as follows:

$$\frac{\partial c}{\partial t} + \mathbf{u}\cdot\nabla c = \operatorname{div}(D_i\nabla c) \text{ in } \Omega_i(t), \quad i = 1,2, \tag{2.6}$$

$$[D_i\nabla c\cdot\mathbf{n}_\Gamma]_\Gamma = 0 \qquad \text{on } \Gamma(t), \tag{2.7}$$

$$c_1 = C_H c_2 \qquad \text{on } \Gamma(t). \tag{2.8}$$

The diffusion coefficient D_i is piecewise constant and in general $D_1 \neq D_2$. The interface condition in (2.7) comes from mass conservation, which implies flux continuity across the interface. The condition in (2.8) is Henry's law, cf. Remark 2. The model has to be completed with suitable initial and boundary conditions for the concentration c.

REMARK 2. Henry's law is a constitutive law describing the balance of chemical potentials at the interface. Under the assumption that kinetic processes at the interface are sufficiently fast, an instantaneous thermodynamical equilibrium is obtained. Henry's law states a linear dependence of the concentration at the interface on the partial pressure in the fluids $p = \beta_i c_i$. The constants β_i, $i = 1,2$ depend on the solute, the solvent and the temperature. The partial pressures from both sides have to coincide. This yields

$$\beta_1 u_1 = \beta_2 u_2 \tag{2.9}$$

	Liquid phase ($\Omega_2 = \Omega_L$)	disperse phase ($\Omega_1 = \Omega_B$)
Density $[kg/m^3]$	1205	1.122
Dynamic viscosity $[Pas]$	0.075	$1.824 \cdot 10^{-4}$
Henry weight β [1]	1	33
diffusion coeff. $[m^2/s]$	$6.224 \cdot 10^{-6}$	$1.916 \cdot 10^{-5}$
surface tension $[N/m]$	0.063	
bubble diameter $[m]$	0.004	

TABLE 2.1
Material parameters for the example considered in this paper.

which results in (2.8) with $C_H = \beta_2/\beta_1$. For further details on the modeling we refer to [13, 28].

2.2. Example of a two-phase flow with mass transport. In this section we describe a concrete example of a two-phase system. The fluid dynamics and mass transport in this system can be accurately described by the models introduced in the previous section. This example will be used in the numerical experiments in secion 8. The example has also been considered in [4, 15, 20, 22].

In a large container filled with a water-glycerol mixture the rise of a $4mm$ air bubble is considered. Initially the shape of the bubble is spherical and the bubble is placed close to the bottom of the container. Both fluids are at rest. Due to buoyancy forces the bubble rises up and deforms during this process until a quasi-stationary state with a fixed ellipsoidal shape and a constant rise velocity is reached. We consider the dissolution process of oxygen from the gaseous phase to the liquid during the rise of the bubble. At the initial state the oxygen concentration inside the liquid mixture is set to zero while the concentration inside the bubble is constant u_0.

In Table 2.1 the material parameters for the considered substance systems are listed. The mixture of water and glycerol consists of 18%(volume) water and 82%(volume) glycerol. The corresponding material data are taken from the literature, cf. [4, 22]. In [22] experimental results for the considered setup are given, however, only with respect to the fluid dynamics.

In order to characterize the predominant effects in flows and specifically two-phase flows the dimensionless numbers Re, Ca and Sc are introduced. The Reynold's number Re describes the ratio between inertia forces and viscous forces within a fluid. For the case of a rising bubble it is defined as

$$Re = \rho_L U_B d_B / \mu_L \tag{2.10}$$

where U_B is a characteristic velocity of the fluid, here the terminal rise velocity of the bubble, and d_B is the (initial) bubble diameter. Note that in the definition of the Reynold's number the fluid properties of the gas phase do not enter. In the considered case we have $Re \approx 7.6$ which says that inertia forces are important for the fluid behavior, but viscosity is still sufficiently high such that the flow can be considered as *laminar*.

Related to the surface tension force the dimensionless capillary number Ca is often

used to characterize the ratio between viscous and surface tension forces:

$$Ca = \mu_L U_B / \tau \tag{2.11}$$

with τ the constant surface tension coefficient of a clean interface. For the system considered here we have a capillary number $Ca \approx 0.14$ which states that the surface tension forces are predominant. The dominance of the surface tension forces implies that the deformation of the bubble shape is moderate and that the resulting bubble shape is stable.

The Reynold's and capillary numbers describe the main characteristics of the fluid flow behavior. For the description of the most important effects of the mass transport in such a two-phase flow system, one typically uses the Schmidt number

$$Sc = \frac{\mu}{\rho D} \tag{2.12}$$

which describes the ratio between kinematic viscosity $\nu = \mu/\rho$ and diffusion D in a fluid. In liquids the diffusion is typically orders of magnitude smaller than the kinematic viscosity leading to high Schmidt numbers in liquid phases. Typical values for Sc in liquids are about 1000. In gaseous phases the Schmidt number is typically of order one. For the dissolution process in the considered example the Schmidt number in the gaseous phase is significantly smaller than in the liquid phase. This is reflected in considerably smaller layers attached to the interface in the liquid phase than in the gaseous phase. The presence of thin boundary layers renders the accurate simulation of mass transport extremely difficult. In [4] instead of the physically correct diffusivity in the liquid, an artificial diffusivity is used to be able to prescribe the Schmidt number. Several Schmidt numbers have been considered to investigate the dependency of the dissolution process on the Schmidt number Sc. Here, we restrict to the case $Sc = 10$ in the liquid phase, for which a thin boundary layer exists the resolution of which is, however, still possible. This corresponds to the material parameters of Table 2.1 (with an artificial value $D_1 = 6.224 \cdot 10^{-6} m^2/s$ for the diffusion coefficient in the liquid phase).

In Fig. 2.1 the rise of the bubble is illustrated. One can capture the main characteristics of the dissolution of oxygen in the liquid phase and the velocity field in terms of streamlines. The results shown are simulation results obtained with discretization techniques discussed below.

Remark 3.
The characteristics of a two-phase flow problem as introduced above depend on the values of the dimensionless numbers Re, Ca and Sc. A further relevant dimensionless number is the Peclet number Pe, which is the ratio of rate of advection of a physical quantity by the flow to the rate of diffusion of the same quantity. The relation $Pe = Re \cdot Sc$ holds. In certain flow regimes there are phenomena that cause a (strong) increase in the numerical complexity of the simulation. We briefly address a few important examples of such phenomena.
Flows with a low Reynold's number (diffusion dominates) are laminar and typically show a much smoother and more stable behavior than flows with a (very) large Reynold's number (convection dominates), which may even become turbulent. Already for one-phase incompressible flows it is well-known that the numerical simulation of laminar flows is significantly easier than that of flows with a large Reynold's number. This obviously carries over to two-phase incompressible flows. Note that in

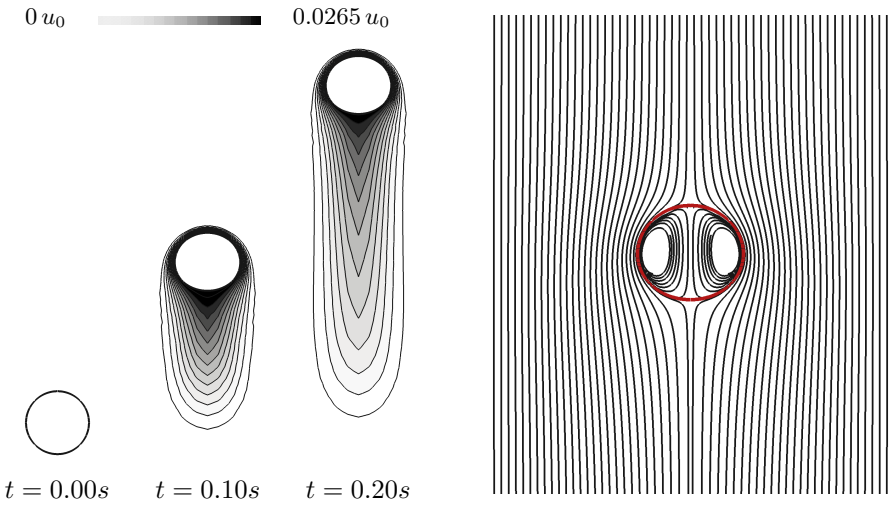

FIG. 2.1. *Concentration contours in the fluid phase at several times for the dissolution process of oxygen from a rising air bubble in a water-glycerol mixture for Schmidt number* $Sc = 10$ *(left) and streamlines around the bubble at* $t = 0.2s$ *(right).*

two-phase flows, depending on the fluid parameters, the Reynold's numbers within the separate phases can be very different.
For a large capillary number Ca, surface tension is small compared to viscous or inertia forces acting on the interface. This typically leads to large deformations of the interface. Such a strong dynamics of the interface is numerically difficult to handle. A small capillary number on the other hand causes other numerical difficulties. These are due to the fact that a small value for Ca corresponds to a large surface tension force which strongly influences the fluid dynamics but is singular in the sense that it acts only on the (evolving) interface.
If in the mass transport problem the Peclet number Pe is very large, this corresponds to a convection-dominated transport problem. Then typically very sharp interior or boundary layers occur, which are difficult to deal with numerically. For laminar flows with a small Reynold's number, say $Re = \mathcal{O}(1)$, the magnitude of the Peclet number is of the same order as that of the Schmidt number, due to the relation $Pe = Re \cdot Sc$. Some specific numerical challenges for two-phase flow simulations are discussed in section 3.

2.3. One-fluid model. As a basis for numerical simulations of two-phase flows one typically does *not* use a model with two Navier-Stokes equations in the two subdomains, as in (2.1), with coupling conditions as in (2.2), (2.3) and a dynamic condition as in (2.4). Instead one very often uses a *one-fluid* model, which we explain in this section. For the numerical *interface representation* different techniques are used in the literature, e.g. the *Volume of Fluid* (VOF) method, the *level set* (LS) method and the *phase field* method. For a treatment of these methods we refer to the literature, e.g. [27, 21, 31, 9]. In this paper we restrict to the level set method, which we briefly explain. At $t = 0$ a *smooth* function $\phi_0(x),\ x \in \Omega$, is chosen, which characterizes the initial interface $\Gamma(0)$ in the following way:

$$\phi_0(x) < 0 \ \Leftrightarrow\ x \in \Omega_1(0), \quad \phi_0(x) > 0 \ \Leftrightarrow\ x \in \Omega_2(0), \quad \phi_0(x) = 0 \ \Leftrightarrow\ x \in \Gamma(0).$$

A popular choice is to take ϕ_0 (approximately) equal to a signed distance function to the initial interface, cf. Fig. 2.2.

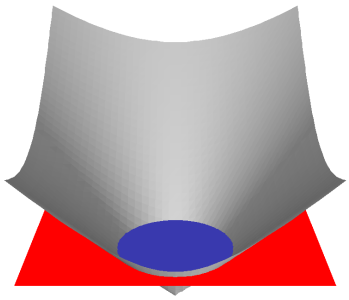

FIG. 2.2. *Initial level set function ϕ_0 equals a signed distance function, 2D example.*

For $t > 0$ the level set function values $\phi(x,t)$ are defined by keeping the values constant along characteristics, induced by the velocity filed $\mathbf{u}$. This results in the transport equation

$$\frac{\partial \phi}{\partial t} + \mathbf{u} \cdot \nabla \phi = 0 \quad \text{in } \Omega,\ t \geq 0, \tag{2.13}$$

which is called the *level set equation*. The interface $\Gamma(t)$ can be characterized by values of the level set function at time t:

$$\Gamma(t) = \{\, x \in \Omega :\ \phi(x,t) = 0 \,\}. \tag{2.14}$$

The level set equation describes the evolution of the interface, hence the condition (2.4) is not needed anymore. The jumps in the coefficients ρ and μ can be described using the level set function ϕ in combination with the Heaviside function $H : \mathbb{R} \to \mathbb{R}$; $H(\zeta) = 0$ for $\zeta < 0$, and $H(\zeta) = 1$ for $\zeta > 0$. For ease one can set $H(0) = \frac{1}{2}$. We define

$$\begin{aligned} \rho(\phi) &:= \rho_1 + (\rho_2 - \rho_1) H(\phi), \\ \mu(\phi) &:= \mu_1 + (\mu_2 - \mu_1) H(\phi). \end{aligned} \tag{2.15}$$

The continuity condition in (2.3) is easy to satisfy by restricting to numerical approximations for the velocity that are continuous. The important stress balance condition (2.2) can be reformulated as a *localized force term in the momentum equation*. Based on these observations the model (2.1)-(2.4) can be reformulated as follows:

$$\begin{cases} \rho(\phi)\big(\dfrac{\partial \mathbf{u}}{\partial t} + (\mathbf{u} \cdot \nabla)\mathbf{u}\big) = \operatorname{div} \boldsymbol{\sigma}(\phi) + \rho(\phi)\mathbf{g} + \delta_\Gamma \operatorname{div}_\Gamma \boldsymbol{\sigma}_\Gamma & \text{in } \Omega, \\ \operatorname{div} \mathbf{u} = 0 \end{cases} \tag{2.16}$$

$$\frac{\partial \phi}{\partial t} + \mathbf{u} \cdot \nabla \phi = 0 \qquad \text{in } \Omega, \tag{2.17}$$

with $\boldsymbol{\sigma}(\phi) := -p\mathbf{I} + \mu(\phi)\big(\nabla \mathbf{u} + (\nabla \mathbf{u})^T\big)$, i.e., $\boldsymbol{\sigma} = \boldsymbol{\sigma}_i$ in $\Omega_i(t)$, and δ_Γ a suitable Dirac delta function that localizes the force $\operatorname{div}_\Gamma \boldsymbol{\sigma}_\Gamma$ on the interface. Note that in (2.16)

we now have *one* Navier-Stokes equation in the whole domain Ω. Hence, this model is called the one-fluid model. Compared to the two Navier-Stokes equations in (2.1) the Navier-Stokes equation in (2.16) is more complicated, due to the discontinuities in viscosity μ and density ρ and the localized interface force term $\delta_\Gamma \operatorname{div}_\Gamma \boldsymbol{\sigma}_\Gamma$. To obtain a well-posed model one has to add suitable boundary and initial conditions for ϕ and $\mathbf{u}$. Note that the initial condition for ϕ determines the initial interface $\Gamma(0)$, due to (2.14). This one-fluid model forms the basis for many numerical simulations of the fluid dynamics in two-phase incompressible flow systems in the literature.

In this paper we restrict to *finite element discretization methods*. For these one needs a suitable *variational formulation* of the partial differential equations. Since in the part on numerical methods below we focus on the mass transport equation, we only treat a variational formulation of the mass transport model (2.6)-(2.8). This is done in section 5. For suitable variational formulations of the one-fluid model, consisting of the Navier-Stokes equations (2.16) and the level set equation (2.17), we refer to the literature, e.g. [9].

3. Numerical challenges. The two-phase flow models introduced above pose enormous challenges to numerical simulation tools. Such flow models can not be solved reliably and accurately by the commercial codes that are available nowadays. Below we address a few causes of the very high numerical complexity of this problem class.

Evolving unknown interface. The interface evolution is determined by the dynamic condition $V_\Gamma = \mathbf{u} \cdot \mathbf{n}_\Gamma$. The interface is a geometric object and it turns out that an accurate numerical approximation of this object and its evolution is a big challenge. In case of geometric singularities (e.g. droplet break up or collision) it becomes even more complicated. An accurate interface approximation is of major importance for the two-phase flow simulation, in particular in systems where the surface tension is a driving force.

Discretization of surface tension force. In many systems the surface tension force has a strong effect on the fluid dynamics. Hence, an accurate discretization of $\operatorname{div}_\Gamma \boldsymbol{\sigma}_\Gamma$ is essential for accurate simulation results. This surface tension force acts only on the (unknown) interface and depends on the curvature of the interface, cf. (2.5). An accurate discretization of the surface tension force turns out to be a very difficult task.

Moving discontinuities. Many quantities are discontinuous across the (evolving) interface. For example, the density and viscosity values have jumps across the interface. Due to surface tension forces the pressure is discontinuous across the interface. The force balance (2.2) and a jump in the viscosity across the interface typically induce a discontinuity across the interface of the normal derivative of the velocity. Due to the Henry condition (2.8) the concentration c is discontinuous across the interface. For an accurate numerical treatment of such moving discontinuities special numerical techniques are required.

Transport processes on moving manifolds. If surfactants are considered, this leads to a transport equation on the (evolving) interface. The numerical solution of partial differential equations on moving manifolds is a difficult topic, which has been addressed in the literature only recently.

Resolution of boundary layers. In many applications boundary layers form at the interface of the two-phase system. The resolution of these boundary layers is very demanding. In [4] the dependency of the boundary layer thickness on the Schmidt number has been investigated for the setting described above and a correlation of the form $Sc^{-0.65} \cdot 0.5mm$ has been observed. The findings in that paper imply a ratio between the bubble diameter and the thickness of the boundary layer of 8 for $Sc = 1$ up to 400 for $Sc = 1000$. Hence, for realistic Schmidt numbers ($Sc \approx 1000$), the resolution of boundary layers with three-dimensional simulation tools is extremely difficult. For these realistic Schmidt numbers the Peclet number $Pe = Re \cdot Sc$ is very large and thus the transport problem is strongly convection dominated, which causes problems with respect to the stability of the finite element discretization. Typically this requires some form of convection stabilization.

Numerical solution of discrete problems. After implicit discretization in time and discretization in space one obtains a very large nonlinear system of equations (for the discrete quantities) in each time step. In simulations by far most of the total computing time is needed for solving these large nonlinear systems. For efficiency reasons one has to use iterative solvers that take advantage of certain structural properties of the problem. Related to the development of such iterative solvers there are many open problems.

Linearization. The flow model contains several strongly nonlinear couplings. In the model (2.16)-(2.17) the transport of the level set function depends on the flow field $\mathbf{u}$. The latter is determined from the Navier-Stokes equation (2.16), but in this equation there is a strong dependence on (the zero level of) the level set function ϕ. This coupling between fluid dynamics, (2.16), and interface evolution, (2.17), is strongly nonlinear. If mass transport is considered and if there is a dependence of τ on the dilute concentration, i. e., $\tau = \tau(c)$, this coupling in two directions between fluid dynamics and mass transport is also in general strongly nonlinear. The same holds for a coupling in two directions between fluid dynamics and surfactant transport, i. e., $\tau = \tau(S)$, where S is the surfactant concentration on the evolving interface. The topic of development of effcient and robust linearization techniques is an important one.

For dealing with these challenges, special numerical approaches have been developed. In the remainder of this paper we treat three numerical techniques in more detail, namely:

- XFEM for nonaligned discontinuities (section 4),
- Nitsche method for interface conditions (section 5),
- Space-time FEM. (section 6).

All three techniques are based on rather general numerical concepts. Our aim is to explain the basic ideas of these concepts and avoid technical details. In section 7 these techniques are combined and result in a very efficient numerical method for the simulation of the mass transport equation. This type of advanced finite element methods for the mass transport equations have been introduced in the literature only very recently, see for instance [16, 17].

4. XFEM for nonaligned discontinuities. In interface capturing methods, like VOF and the level set method, the interface is given implicitly and typically *not*

aligned with the grid or triangulation that is used in the discretization of the flow variables. This *nonalignment* causes severe difficulties for the discretization methods, because certain important quantities (pressure, solute concentration) are discontinuous across the interface. In the past decade, in the finite element literature the extended finite element method (XFEM), also called cut finite element method, has been developed to overcome these difficulties. There is an extensive literature on the XFEM, cf. [6, 8, 26, 10, 12] and the references therein. We outline the basic idea of this technique for the approximation of the discontinuous solutions such as the pressure p or the solute concentration c.

It is known that the approximation of a smooth function with a discontinuity across the nonaligned interface with piecewise polynomials gives only poor approximation results. The approximation error (in the L^2 norm) scales with $\sqrt{h}$ independent of the polynomial degree. To overcome this, we introduce a special finite element space. The main idea is depicted in Fig. 4.1. We first consider the simpler problem of

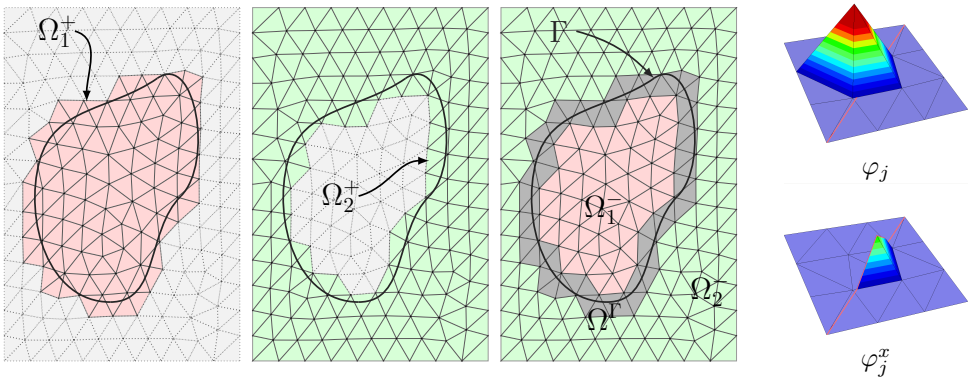

FIG. 4.1. *Extended finite element space as a sum of fictitious domain spaces (left) and sketch of a standard and an extended basis function (right), 2D example.*

approximating a function w_1 in the domain Ω_1. The function in Ω_1 has a smooth extension $\tilde{w}_1$ into Ω_1^+, the domain of all elements (triangles in Fig. 4.1) which have some part in Ω_1. For the approximation of this smooth extension $\tilde{w}_1$ we use standard piecewise linears in Ω_1^+ and obtain the usual good approximation of $\tilde{w}_1$ and thereby also of w_1. We apply the same procedure on Ω_2^+ and can thus construct a good approximation of a smooth function w which is discontinuous across Γ. For this procedure we need one degree of freedom per vertex except for vertices in Ω^Γ, the domain of elements which are intersected by the interface. Here, we need two degrees of freedom per vertex, one for each domain (Ω_1^+ and Ω_2^+). The corresponding finite element space is

$$Q_h^\Gamma = \mathcal{R}_1 Q_h \oplus \mathcal{R}_2 Q_h$$

with Q_h the finite element space of piecewise linears and $\mathcal{R}_i$ the restriction operator to Ω_i. Note that $\dim(\mathcal{R}_i Q_h)$ coincides with the number of vertices in Ω_i^+. This finite element space and especially its dimension depends on the location of the interface Γ.

The finite element space Q_h^Γ can also be characterized as an extension of the standard finite element space Q_h, i.e., $Q_h^\Gamma = Q_h \oplus Q_h^x$, with a suitable space Q_h^x, which is

spanned by so-called enrichment functions. We explain how the basis functions of Q_h^x are constructed. To this end, consider a basis function $\varphi_j \in Q_h$ corresponding to a vertex $\mathbf{x}_j$ in Ω^Γ. Without loss of generality assume the vertex $\mathbf{x}_j$ lies in Ω_1. Then we define the enrichment function $\varphi_j^x = \mathcal{R}_2\varphi_j$. For a vertex in Ω_2 we accordingly define $\varphi_j^x = \mathcal{R}_1\varphi_j$. This choice gives the locality property of the new basis functions $\varphi_j^x(\mathbf{x}_k) = 0$ for all vertices $\mathbf{x}_k$. The basis functions φ_j and φ_j^x corresponding to a vertex $\mathbf{x}_j$ in Ω^Γ are depicted in Fig. 4.1 (right) for a 2D example. In practice the interface Γ is replaced by a numerical approximation Γ_h.

This XFEM has been succesfully applied in the simulation of two-phase flow fluid dynamics. We illustrate this for a toluene-water rising droplet system. The results are taken from [9] and illustrate the effect of using the XFEM instead of a standard FEM for discretization of the pressure variable. We refer to section 7.11.2 in [9] for a precise description of the flow system and the numerical solver components used. The pressure is either discretized using the XFEM space $Q_h^{\Gamma_h}$ or the standard finite element space Q_h consisting of piecewise linears. Fig. 4.2 shows the initial shape of the droplet and the droplet shapes after 10 time steps for both cases.

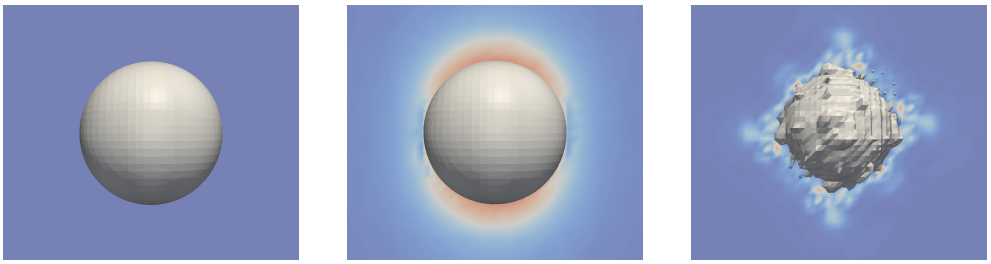

FIG. 4.2. *Initial droplet shape (left) and after 10 time steps for the XFEM case (middle) and the standard FEM case (right).*

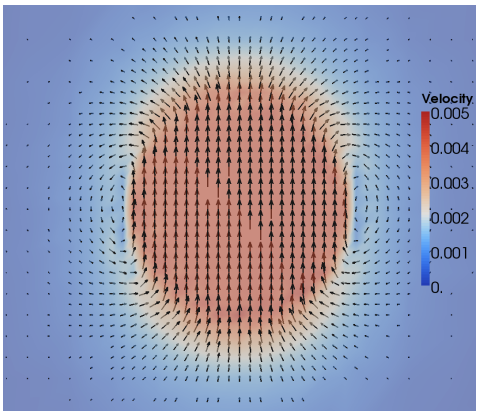

FIG. 4.3. *Velocity field at interface for the XFEM case.*

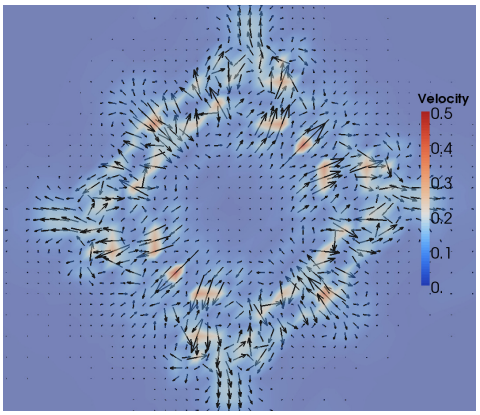

FIG. 4.4. *Velocity field at interface for the standard FEM case.*

While the interface is smooth using the extended pressure finite element space, it shows many "spikes" in the case of the standard pressure space. These spikes are of course non-physical and only caused by numerical oscillations at the interface, so-called *spurious velocities*, which are shown in Fig. 4.4. The velocity field for the

XFEM case is smooth showing the characteristic vortices, cf. Fig. 4.3. Note that the scaling of the color coding in both figures is very different, with a maximum velocity of $5 \cdot 10^{-3}\, m$ for the extended pressure space compared to $5 \cdot 10^{-1}\, m$ for the standard pressure space. These results clearly show, that for this realistic two-phase flow example the standard pressure space Q_h is not suitable, whereas the extended pressure space $Q_h^{\Gamma_h}$ yields satisfactory results.

In the numerical simulations of two-phase flows presented in this paper we use the XFEM for the discretization of the (discontinuous) pressure variable and the (discontinuous) solute concentration c. In the literature one can also find extended finite element techniques for the discretization of the velocity, which is nonsmooth across the interface because it has a kink behavior. Such a so-called kink enrichment method for the velocity is treated in e.g. [8]. In the simulation of the two-phase fluid dynamics, however, such an enrichment of the velocity finite element space is not often used in practice, cf. [8] for an explanation of this.

REMARK 4. The finite element space $Q_h^{\Gamma_h}$ depends on the location of the interface Γ_h. Thus, if the interface evolves the finite element space Q_h^{Γ} and its dimension changes. This causes difficulties for the numerical treatment of unsteady problems. A solution to this is discussed in section 6.

REMARK 5. The use of the XFEM enrichment functions, which results in an accurate discretization, causes problems for the solution of the linear system arising from the discretization. The key problem is that the conditioning of the resulting matrix depends on the position of the interface with respect to the triangulation. To overcome this problems stabilization techniques have been introduced in [5, 12, 32]. For the discretization of a (Navier-)Stokes problem with an enrichment of the pressure space a stabilization is used to guarantee LBB-stability for the pair of finite element spaces in [12]. In [5, 32] stabilized discretizations for interface problems as they appear for mass transport problems are discussed. In [18] it is shown that for the solution of mass transport problems *optimal* iterative strategies can be designed without additional stabilizations.

5. Nitsche method for interface conditions. The Nitsche method is a general finite element technique for enforcing boundary or interface conditions in a weak sense. The technique can be used in different applications, cf., e.g. [10, 11]. In this section we explain the basic idea of the Nitsche method for the mass transport problem (2.6)-(2.8) for the case that the interface is *stationary*. The method allows an accurate and convenient treatment of the Henry interface condition. The generalization to the case of an evolving interface is briefly addressed in section 7.

The Nitsche method can only be applied in a variational setting. Therefore, we first need a well-posed variational formulation of the mass transport equation. The Henry condition can be reformulated in the form $[\beta c]_{|\Gamma} = 0$, with a suitable piecewise constant $\beta_i > 0$ in Ω_i, $i = 1, 2$. We assume that the velocity field $\mathbf{u}$ is given. Furthermore, for simplicity we assume that the dilute concentration has to satisfy the homogeneous boundary condition $c = 0$ on $\partial\Omega$. For the variational formulation we need suitable scalar products and (Sobolev) spaces. Here we outline the key components, details are given in section 10.2 in [9]. We define a function space

$$V := \{\, v \in L^2(\Omega) \,:\, v_{|\Omega_i} \in H^1(\Omega_i),\ i = 1, 2,\ v_{|\partial\Omega} = 0,\ [\beta v]_{|\Gamma=0} \,\}.$$

It is important to note that the Henry condition is put as an essential condition in the definition of this space. On V we use the weighted scalar products

$$(u,v)_0 := (\beta u, v)_{L^2} = \int_\Omega \beta uv\, dx, \qquad (u,v)_{1,\Omega_1\cup\Omega_2} := \sum_{i=1}^{2} \beta_i \int_{\Omega_i} \nabla u_i \cdot \nabla v_i\, dx$$

Related to the transport problem we define the bilinear form

$$a(u,v) := (Du,v)_{1,\Omega_1\cup\Omega_2} + (\mathbf{u}\cdot\nabla u, v)_0, \quad u,v \in V. \tag{5.1}$$

Here D denotes the piecewise constant diffusion coefficient. A suitable variational formulation of the mass transport problem, with a source term f, is as follows: determine $c = c(\cdot,t) \in V$ such that for $t \in [0,T]$

$$(\frac{\partial c}{\partial t}, v)_0 + a(c,v) = (f,v)_0 \quad \text{for all} \quad v \in V \tag{5.2}$$

holds. The derivative $\frac{\partial c}{\partial t}$ is defined in a suitable weak sense (not specified here). It can be shown that this is a well-posed weak formulation of the mass transport equation.

We introduce a Nitsche based finite element discretization of this problem. We assume that the interface is nonaligned, and therefore one has to be careful with the choice of the finite element space. In section 4 it is explained that the XFEM space Q_h^Γ is a suitable finite element space for the discontinuous dilute concentration c. It is very difficult (often even impossible), in particular for the case of an evolving interface, to incorporate the Henry interface condition $[\beta c]_{|\Gamma}$ in this finite element space. The Nitsche technique allows us to use the space Q_h^Γ *without* the Henry interface condition. The Henry condition is enforced, in a weak sense, by changing the bilinear form in the variational problem. Before we introduce this modified bilinear form we need a suitable averaging of functions across the interface. We consider a triangulation $\mathcal{T}_h$ consisting of tetrahedra T, with $h_T := \mathrm{diam}(T)$ and $h := \max\{\, h_T : T \in \mathcal{T}_h \,\}$. For any tetrahedron $T \in \mathcal{T}_h$ let $T_i := T \cap \Omega_i$ be the part of T in Ω_i. We define the weighted average

$$\{v\} := \kappa_1 (v_1)_{|\Gamma} + \kappa_2 (v_2)_{|\Gamma}, \quad (\kappa_i)_{|T} := \frac{|T_i|}{|T|}, \tag{5.3}$$

where v_i denotes the restriction of a function v to Ω_i. We now introduce the modification of the bilinear form in (5.1):

$$\begin{aligned} &a_h(u,v) := (Du,v)_{1,\Omega_1\cup\Omega_2} + (\mathbf{u}\cdot\nabla u, v)_0 + N_h^\Gamma(u,v) \text{ with} \\ &N_h^\Gamma(u,v) := -([\beta u], \{D\nabla v\cdot\mathbf{n}_\Gamma\})_\Gamma - (\{D\nabla u\cdot\mathbf{n}_\Gamma\}, [\beta v])_\Gamma + \lambda h^{-1}([\beta u],[\beta v])_\Gamma, \end{aligned} \tag{5.4}$$

with $\lambda > 0$ a parameter. Here $(\cdot,\cdot)_\Gamma$ denotes the L^2 scalar product on the interface Γ (in practice replaced by an approximation Γ_h). In this modified bilinear form the term $(\{D\nabla u\cdot\mathbf{n}_\Gamma\}, [\beta v])_\Gamma$ is added for consistency reasons, the term $([\beta u], \{D\nabla v\cdot\mathbf{n}_\Gamma\})_\Gamma$ is included to maintain symmetry and the term $\lambda h^{-1}([\beta u],[\beta v])_\Gamma$ is used because we want to satisfy the Henry condition $[\beta c]_{|\Gamma} = 0$ (approximately). The latter term penalizes the jump $[\beta u]_{|\Gamma}$. An important property of this Nitsche method is that the penalty term is consistent: it vanishes if we insert the solution c of the continuous

problem. The Nitsche-XFEM discretization of the mass transport problem (5.2) is as follows: determine $c_h = c_h(\cdot,t) \in Q_h^\Gamma$ such that for $t \in [0,T]$

$$(\frac{\partial c_h}{\partial t}, v_h)_0 + a_h(c_h, v_h) = (f, v_h)_0 \quad \text{for all} \quad v_h \in Q_h^\Gamma. \tag{5.5}$$

In practice the integrals (and average) over Γ that occur in this equation are replaced by the corresponding ones over Γ_h. Note that (5.5) is a discretization only w.r.t. the space variable. The time discretization can be realized by some finite differencing (method of lines). In section 6 we explain an alternative for this "first space then time discretization" approach which is also suitable for the case where the interface is *not stationary*. Again, we emphasize that the Henry condition is not built into the finite element space Q_h^Γ, but weakly enforced by a suitable modification of the bilinear form. The performance of the method turns out to be rather robust w.r.t. the choice for the stabilization parameter λ. Error analysis for this method has been developed and yields that for the discrete solution c_h an optimal error bound of the form $\|c(\cdot,t) - c_h(\cdot,t)\|_{L^2(\Omega)} \leq ch^2$ holds [23]. Also bounds for the error in the Henry condition are available and of the form $\|[\beta c_h(\cdot,t)]_\Gamma\|_\Gamma \leq ch^{3/2}$.

6. Space-time formulation of parabolic problems. The solution of problems with moving interfaces in an Eulerian framework is challenging. Between time steps some degrees of freedom switch phases. The derivation of appropriate discrete equations for these unknowns is not straightforward. The solution can be discontinuous across the interface. Hence, an approximation of the time derivative by some kind of finite difference stencil, as it is typically done in the method of lines, is not feasible. One way to deal with this problem is a formulation in space-time. The domain and the time interval define a so-called time slab on which the new formulation of the problem is derived. In the space-time setting the (space-time) interface is stationary and the time derivate can naturally be defined within the separate space-time subdomains.

We explain the basic concept of the space-time finite element method for a simpler problem with a *smooth* solution, namely the parabolic model problem

$$\begin{aligned} \frac{\partial u}{\partial t} - \Delta u &= f \quad \text{in } \Omega,\ t \in [0,T], \\ u(\cdot,0) &= u_0 \quad \text{in } \Omega, \\ u(\cdot,t) &= 0 \quad \text{on } \partial\Omega. \end{aligned} \tag{6.1}$$

For simplicity we assume f to be independent of t. We use a partitioning of the time domain $0 = t_0 < t_1 < \ldots < t_N = T$, with a fixed time step size $\Delta t = T/N$, i. e., $t_j = j\Delta t$. This assumption of a fixed time step is made to simplify the presentation, but is *not* essential for the method. Corresponding to each time interval $I_n := (t_{n-1}, t_n)$ we have a consistent triangulation $\mathcal{T}_n$ of the domain Ω. This triangulation may vary with n. Let V_n be a finite element space of continuous piecewise polynomial functions corresponding to the triangulation $\mathcal{T}_n$, with boundary values equal to zero. For $1 \leq n \leq N$ and a nonnegative integer k we define, on each time slab $Q^n := \Omega \times I_n$, a space-time finite element space as follows:

$$V_{kn} := \left\{ v : Q^n \to \mathbb{R} :\ v(x,t) = \sum_{j=0}^{k} t^j \phi_j(x),\ \phi_j \in V_n \right\}, \tag{6.2}$$

for $1 \leq n \leq N$. The corresponding space-time discretization of (6.1) reads: Determine u_h such that for all $n = 1, 2, \ldots, N$, $(u_h)_{|Q^n} \in V_{kn}$ and

$$\begin{aligned} &\int_{t_{n-1}}^{t_n} \big(\frac{\partial u_h}{\partial t}, v_h\big)_{L^2} + (\nabla u_h, \nabla v_h)_{L^2}\, dt + ([u_h]^{n-1}, v_h^{n-1,+})_{L^2} \\ &= \int_{t_{n-1}}^{t_n} (f, v_h)_{L^2}\, dt \quad \text{for all } v_h \in V_{kn}, \end{aligned} \tag{6.3}$$

where $(\cdot,\cdot)_{L^2} = (\cdot,\cdot)_{L^2(\Omega)}$,

$$[w_h]^n = w_h^{n,+} - w_h^{n,-}, \quad w_h^{n,+(-)} = \lim_{s \to 0^{+(-)}} w_h(\cdot, t_n + s),$$

and $u_h^{0,-} \in V_1$ an approximation of the initial data u_0. Such space-time finite element methods for parabolic problems are well-known in the literature. For an analysis and further explanation of this discretization method we refer to the literature, e.g. [30].

As examples, we consider two important special cases, namely $k = 0$, $k = 1$. If $k = 0$ then $v_h \in V_{kn}$ does not depend on t. Define $u_h^n(x) := u_h(x,t)$, $t \in I_n$. The method (6.3) for determining $u_h^n \in V_n$ reduces to the implicit Euler scheme:

$$\frac{1}{\Delta t}(u_h^n - u_h^{n-1}, v_h)_{L^2} + (\nabla u_h^n, \nabla v_h)_{L^2} = (f, v_h)_{L^2} \quad \text{for all } v_h \in V_n.$$

We now consider $k = 1$. Then on Q^n the function u_h^n can be represented as $u_h^n(x,t) = \hat{u}_h^n(x) + \frac{1}{\Delta t}(t - t_{n-1})\tilde{u}_h^n(x)$, with $\hat{u}_h^n$, $\tilde{u}_h^n \in V_n$. These unknown functions are uniquely determined by the coupled system

$$\begin{aligned} (\hat{u}_h^n + \tilde{u}_h^n, v_h)_{L^2} + \Delta t\big(\nabla \hat{u}_h^n + \frac{1}{2}\nabla \tilde{u}_h^n, \nabla v_h\big)_{L^2} &= (u_h^{n-1,-}, v_h)_{L^2} + \Delta t (f, v_h)_{L^2}, \\ \frac{1}{2}(\tilde{u}_h^n, v_h)_{L^2} + \Delta t\big(\frac{1}{2}\nabla \hat{u}_h^n + \frac{1}{3}\nabla \tilde{u}_h^n, \nabla v_h\big)_{L^2} &= \frac{1}{2}\Delta t (f, v_h)_{L^2}, \end{aligned} \tag{6.4}$$

for all $v_h \in V_n$, cf. [30]. Note that although the discretization is in $d+1$ dimension, if d is the dimension of the spatial domain, the method has a time-stepping structure such that the computational complexity essentially depends (only) on the dimension of the underlying spatial finite element space V_n. The considered method is often called a Discontinuous Galerkin (DG) method (in time) as the space-time finite element space does not ensure continuity in time in a strong sense, but only in a weak sense. As a time integration method the space-time DG method is stable and has good smoothing properties. The big advantage, however, is the great flexibility that comes with the space-time formulation. This flexibility is used to incorporate the more difficult case where for instance diffusion coefficients are discontinuous across a moving interface and the finite element space is no longer independent of time. We explain this in the next section.

7. Space-time Nitsche-XFE method. The discretization of a parabolic problem with a moving interface is significantly more difficult than for the model problem discussed before. We apply the concepts of the XFEM space and the Nitsche technique in a *space-time setting*, which results in a suitable discretization method for the mass transport problem with a moving interface. We only sketch the components of such a discretization and refer to [17] for details.

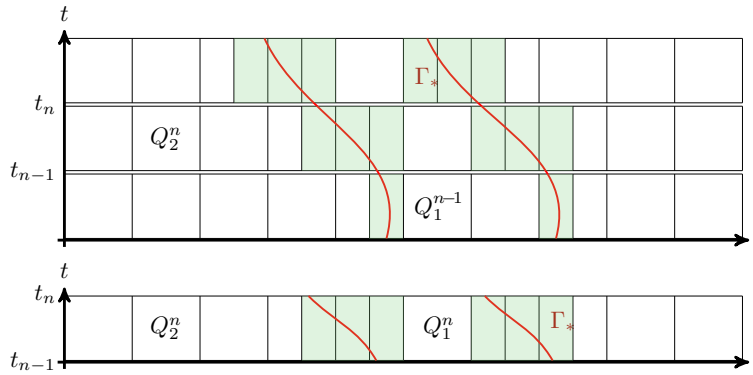

FIG. 7.1. *Sketch of space time slabs and relevant areas for the space-time XFEM.*

In order to capture the moving discontinuities a generalization of the enrichment procedure of the XFEM space as described in section 4 is needed. We take $k = 1$ (linear finite elements) in (6.2) and apply the enrichment procedure on a space-time slab, cf. Fig. 7.1. In the enrichment special discontinuous space-time basis functions, which depend on the interface position in space-time, are added to the original finite element space V_{1n}. This is depicted in Fig. 7.1: the marked space-time elements are cut by the (space-time) interface and corresponding to *every* degree of freedom in these elements an enrichment function is added. This can lead to a different number of unknowns on different time slabs. This, however, is not a problem due to the weak coupling introduced by the Discontinuous Galerkin formulation in time.

The (weak) enforcement of the interface condition for the stationary interface as described in section 5 has a straightforward extension to the space-time domain. The corresponding contribution of the Nitsche integrals takes the form $\int_{t_{n-1}}^{t_n} N_h^{\Gamma(t)}(u,v)\,dt$, with $N_h^{\Gamma(t)}$ as in (5.4).

The resulting discrete problem does not allow for a block structure as in (6.4) where only *space* integrals have to evaluated. This is due to the fact that the problem parameters D and β as well as the ansatz and test function depend on space *and time*. Instead, integration on *space-time geometries* has to be used.

REMARK 6. Due to the discontinuous coefficients and shape functions the space-time formulation is posed on space-time subdomains $Q_i^n = \bigcup_{t\in[t_{n-1},t_n]} \Omega_i(t)$. To implement a method with integrals of the form $\int_{Q_i^n} \cdot\, dxdt$ one needs special strategies for the numerical integration. We do not discuss this here but refer to [16] for more information on this.

To summarize, a very efficient and accurate finite element discretization of the mass transport problem (2.6)-(2.8) is obtained, by using a variational formulation in *space-time* in which the Henry condition is treated by the *Nitsche technique* and the finite element space is built by the *space-time XFEM*. A rigorous error analysis of this method, resulting in second order error bounds both with respect to the space and time mesh size, is given in [17].

8. Numerical simulation of mass transport problem. We discuss the results of numerical simulations of the two-phase flow system described in section 2.2. The simulation of the fluid dynamics of this flow problem has also been considered in [20, 4, 15]. The numerical simulation including mass transport, with $Sc = 10$, has further been investigated in [4, 15]. For the fluid dynamics of the system experiments have been carried out in [22]. The methods described above are implemented in the software package DROPS, cf. [7]. For the rise velocity and the pathlength of the barycenter of the bubble we get values of $0.112m/s$ and $21.44mm$, respectively. The final shape of the bubble has an aspect ratio of maximum height to maximum width of 0.88. All three values are in good agreement with the numerical and experimental results in [4, 15, 20, 22]. Based on this and a systematic validation study of fluid dynamics simulations with DROPS in [3, 19] we conclude that the flow field obtained with DROPS is sufficiently accurate to serve as a reliable input for the simulation of the mass transport problem, which we discuss next.

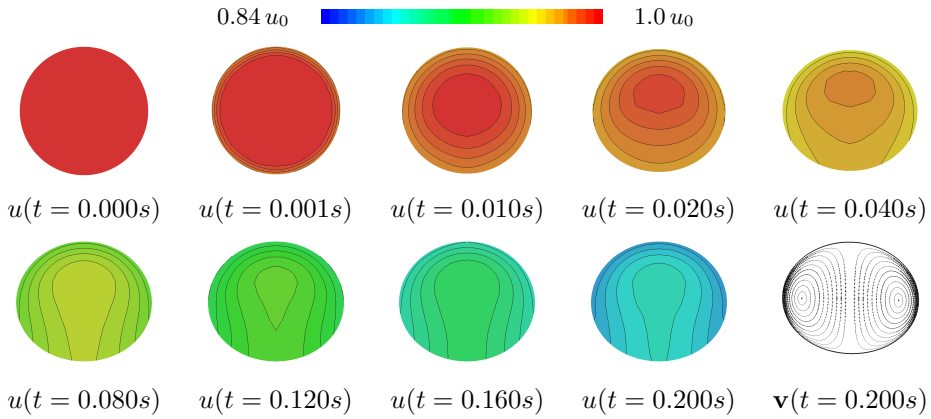

FIG. 8.1. *Concentration distribution inside the gaseous bubble.*

We consider the numerical solution of the described system with a discretization combining the space-time formulation, the extended finite element technique (in space-time) and the Nitsche method. Piecewise linear functions in space and time are used and a Nitsche stabilization parameter $\lambda = 20$. In Fig. 2.1 the evolution of concentration isolines in the liquid for the simulation at different time stages is shown. The corresponding concentration fields inside the bubble at different times and the streamlines corresponding to the velocity (relative to the bubble rise velocity) at $T = 0.2$ are shown in Fig. 8.1. Note that the scalings in Fig. 2.1 and Fig. 8.1 are very different due to the large Henry number.

In Fig. 8.2 we consider the concentration along straight lines which are crossing the center of the bubble at $T = 0.2$. We consider the line through the tip of the bubble ($0°$), a line through the equator ($90°$) and one line at a $135°$ angle from the tip. On those lines we plotted the concentration. Due to the Henry interface condition the concentration has jumps across the interface such that the concentration inside the bubble is 33 times larger than outside. We adapted the scaling for the concentration inside and outside the bubble. The scaling is chosen such that a continuous line in the plot corresponds to a concentration field fulfilling the Henry interface condition. We observe in the plot that this condition is fulfilled very accurately. We considered the data given in [15, Figure 9.35] for a comparison. The results are in good

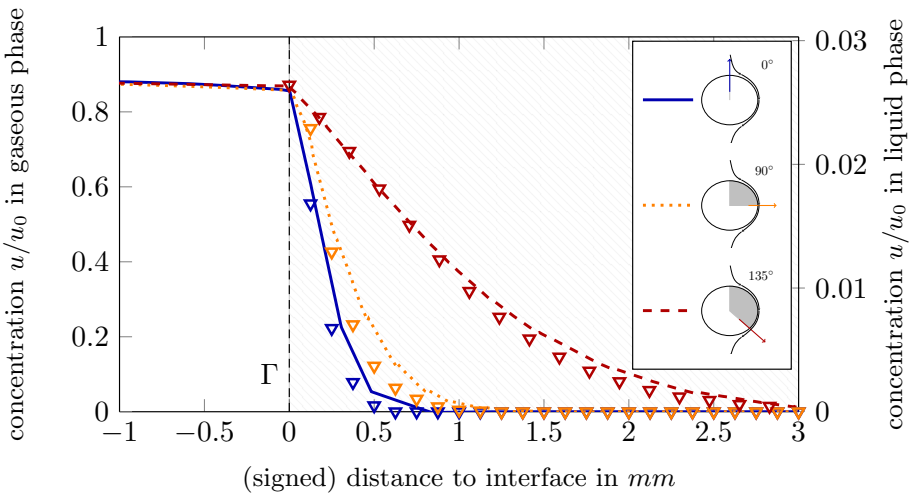

FIG. 8.2. *Concentration along lines for angles* 0°, 90° *and* 135° *computed with* DROPS *(lines) and comparison data from [15] (triangles).*

agreement.

The two-phase flow problem considered in this section has a dynamically evolving and deforming interface with a complex flow structure and a convection-dominated transport of the solute. The finite element techniques used in the simulation of the fluid dynamics and the solute transport provide an efficient solution strategy which has been proven to be robust with respect to the interface position an the moving discontinuities. This can be concluded from the results presented above and from other simulation studies with the DROPS package, cf. [7]. The techniques are flexible, in the sense that these can be combined with adaptivity concepts (local grid refinement close to the interface) and with higher order discretizations. This flexibility and the fact that for the space-time Nitsche-XFEM for the mass transport problem there is a rigorous second order error bound available, are advantages of this approach compared to the finite volume based method used in [15].

9. Conclusion and outlook. In this paper we outlined important numerical challenges in the numerical simulation of sharp interface models for two-phase incompressible flows. Three important and relatively new finite element techniques (XFEM, Nitsche, space-time FEM) are explained and combined for the discretization of the mass transport equation. As far as we know, the resulting space-time Nitsche-XFE method is the only Eulerian discretization method for this type of solute transport equation which has a proven second order accuracy.
In our opinion the development of satisfactory numerical simulation tools for two-phase incompressible flows is still in its infancy. Hence an outlook discussion can be very extensive. Here we restrict ourselves to a few brief comments on topics for further research.
We applied the space-time XFEM approach to the solute transport equation. The application of the space-time technique for the simulation of the fluid dynamics problem (Navier-Stokes model) appears to be a promising approach. This, however, has not been studied in the literature so far and is a topic of current research.
Almost nothing is known concerning accurate simulation of two-phase flows with more

complex interfacial rheology, for example, Newtonian bulk fluids with interfaces that have (due to surfactants on nano-particles) viscous or visco-elastic behavior. Such systems are very important in applications, cf. [24, 25].
We are not aware of any literature in which numerical methods for a realistic model of solute transport combined with reaction processes are studied.
A general key difficulty in this field is the validation of numerical methods. Only very few papers are available, cf. [19], in which benchmark results for two-phase flow simulations are presented.
For laminar *one*-phase incompressible flows there is an extensive literature on error analyses of finite element discretization methods. For two-phase incompressible flows (almost) no rigorous discretization error analysis is known.
Time and space discretization results in a very large and strongly nonlinear system of equations for the discrete unknowns. If one applies standard (black box) iterative solvers, the computing times, even on modern architectures, are unacceptable. Hence, special solution methods, that make use of problem specific structures are needed. Such solvers are not avaible, yet.
Discrete linear systems arising from discretizations of two-phase flows are already challenging due to high contrasts in material parameters (density, viscosity, diffusivity). If additionally non-standard components such as extended finite element or space-time finite element spaces come into play, the iterative solution of linear systems gets extremely difficult. Only for special cases satisfying solution strategies are known in the litature, e.g. [5, 12, 18].

Acknowledgement. The authors gratefully acknowledge funding by the German Science Foundation (DFG) within the Priority Program (SPP) 1506 "Transport Processes at Fluidic Interfaces".

REFERENCES

[1] S. Aland, J. Lowengrub, and A. Voigt, *A continuum model of colloid stabilized interfaces*, Physics of Fluids, 23 (2011), p. 062103.
[2] D. Anderson, G. McFadden, and A. Wheeler, *Diffusive-interface methods in fluid mechanics*, Annu. Rev. Fluid Mech., 30 (1998), pp. 139–165.
[3] E. Bertakis, S. Gross, J. Grande, O. Fortmeier, A. Reusken, and A. Pfennig, *Validated simulation of droplet sedimentation with finite-element and level-set methods*, Chemical Eng. Science, 65 (2010), pp. 2037–2051.
[4] D. Bothe, M. Koebe, and H.-J. Warnecke, *VOF-simulations of the rise behavior of single air bubbles with oxygen transfer to the ambient liquid*, in Transport Phenomena with Moving Boundaries, F.-P. Schindler, ed., VDI-Verlag, Düsseldorf, 2004, pp. 134–146.
[5] E. Burman and P. Hansbo, *Fictitious domain finite element methods using cut elements: II. a stabilized Nitsche method*, Appl. Num. Math., 62 (2012), pp. 328 – 341. Third Chilean Workshop on Numerical Analysis of Partial Differential Equations (WONAPDE 2010).
[6] J. Chessa and T. Belytschko, *An extended finite element method for two-phase fluids*, ASME Journal of Applied Mechanics, 70 (2003), pp. 10–17.
[7] *DROPS package for simulation of two-phase flows.* `http://www.igpm.rwth-aachen.de/DROPS/`.
[8] T. Fries and T. Belytschko, *The generalized/extended finite element method: An overview of the method and its applications*, Int. J. Numer. Meth. Engrg., 84 (2010), pp. 253–304.
[9] S. Gross and A. Reusken, *Numerical Methods for Two-phase Incompressible Flows*, Springer, Heidelberg, 2011.
[10] A. Hansbo and P. Hansbo, *An unfitted finite element method, based on Nitsche's method, for elliptic interface problems*, Comp. Methods Appl. Mech. Engrg., 191 (2002), pp. 5537–5552.
[11] P. Hansbo, *Nitsche's method for interface problems in computational mechanics*, GAMM-Mitt., 28 (2005), pp. 183–206.

[12] P. Hansbo, M. Larson, and S. Zahedi, *A cut finite element method for a Stokes interface problem*, Applied Numerical Mathematics, 85 (2014), pp. 90–114.
[13] M. Ishii, *Thermo-Fluid Dynamic Theory of Two-Phase Flow*, Eyrolles, Paris, 1975.
[14] D. Jacqmin, *Calculation of two-phase Navier-Stokes flows using phase-field modeling*, J. Comp. Phys., 155 (1999), pp. 96–127.
[15] M. Koebe, *Numerische Simulation aufsteigender Blasen mit und ohne Stoffaustausch mittels der Volume of Fluid (VOF) Methode*, PhD thesis, Universität Paderborn, 2004.
[16] C. Lehrenfeld, *The Nitsche XFEM-DG space-time method and its implementation in three space dimensions*, Tech. Report 377, IGPM, RWTH Aachen, October 2013. accepted for publication in SIAM J. Sci. Comput.
[17] C. Lehrenfeld and A. Reusken, *Analysis of a Nitsche XFEM-DG discretization for a class of two-phase mass transport problems*, SIAM J. Numer. Anal., 51 (2013), pp. 958–983.
[18] C. Lehrenfeld and A. Reusken, *Optimal preconditioners for Nitsche-XFEM discretizations of interface problems*, Tech. Report 406, IGPM, RWTH Aachen, Aug. 2014. submitted to Num. Math.
[19] H. Marschall, S. Boden, C. Lehrenfeld, C. Falconi, U. Hampel, A. Reusken, M. Worner, and D. Bothe, *Validation of interface capturing and tracking techniques with different surface tension treatments against a Taylor bubble benchmark problem*, Computers and Fluids, 102 (2014), pp. 336–352.
[20] A. Onea, *Numerical simulation of mass transfer with and without first order chemical reaction in two-fluid flows*, PhD thesis, Forschungszentrum Karlsruhe, September 2007.
[21] S. Osher and R. Fedkiw, *Level Set Methods and Dynamic Implicit Surfaces*, Applied Mathematical Sciences,Vol. 153, Springer, Berlin, Heidelberg, New York, 2003.
[22] F. Raymond and J.-M. Rosant, *A numerical and experimental study of the terminal velocity and shape of bubbles in viscous liquids*, Chem. Eng. Sci., 55 (2000), pp. 943–955.
[23] A. Reusken and T. Nguyen, *Nitsche's method for a transport problem in two-phase incompressible flows*, J. Fourier Anal. Appl., 15 (2009), pp. 663–683.
[24] L. Sagis, *Dynamic properties of interfaces in soft matter: experiments and theory*, Rev. Mod. Phys., 83 (2011), p. 1367.
[25] ———, *Modeling interfacial dynamics using nonequilibrium thermodynamics frameworks*, This issue, (2013).
[26] H. Sauerland and T. Fries, *The extended finite element method for two-phase and free-surface flows: A systematic study*, J. Comp. Phys., 230 (2011), pp. 3369–3390.
[27] J. Sethian, *Level Set Methods and Fast Marching Methods*, Cambridge University Press, 1999.
[28] J. Slattery, L. Sagis, and E.-S. Oh, *Interfacial Transport Phenomena*, Springer, New York, second ed., 2007.
[29] K. Teigen, X. Li, J. Lowengrub, F. Wang, and A. Voigt, *A diffusion-interface approach for modelling transport, diffusion and adsorption/desorption of material quantities on a deformable interface*, Comm. Math. Sci., 7 (2009), pp. 1009–1037.
[30] V. Thomee, *Galerkin Finite Element Methods for Parabolic Problems*, Springer, Berlin, 1997.
[31] G. Tryggvason, R. Scardovelli, and S. Zaleski, *Direct Numerical Simulations of Gas-Liquid Multiphase Flows*, Cambridge University Press, Cambridge, 2011.
[32] S. Zahedi, E. Wadbro, G. Kreiss, and M. Berggren, *A uniformly well-conditioned, unfitted Nitsche method for interface problems: Part I*, BIT Numerical Mathematics, 53 (2013), pp. 791–820.